Body-World Interaction (BoWI)

V. 1. Antennas and propagation for BoWI project

PhD student: Rizwan Masood
Thesis Director: Prof. Christian Person
Supervisor: Prof. Ronan Sauleau
Laboratory: Lab-STICC

Thesis Inscription year: 2013
Expected completion of Thesis: 2016

1. Introduction

This PhD thesis is part of the BoWI project which stands for Body-World Interaction. This project is supported by the Labex CominLabs, France and is actually inspired from Body Area Network(s) (BAN). The principle goal of the BoWI project is an accurate gesture and body movement estimation using miniature, low-power and wearable wireless sensor nodes. These sensors are powered by inertial measurement unit(s) (IMU) to extract the information of velocity, orientation, and position using devices such as accelerometers, magnetometers, gyroscopes and antennas and further using this information for 3D reconstruction of the human actor wearing the BoWI network. This idea opens new vistas to develop number of new features and usages for number of exciting and innovative applications while interacting using bodily gestures with a plethora of smart environments such as home, media, information systems, entertainment and health systems. This will also influence all existing motion capture technologies which are mostly composed of several cumbersome devices along with the high cost constraint. BoWI is focused on the society challenge called Digital Environment for the Citizen and the social challenge of ICT for personalized medicine and is composed of a multidisciplinary research consortium from different French research laboratories.

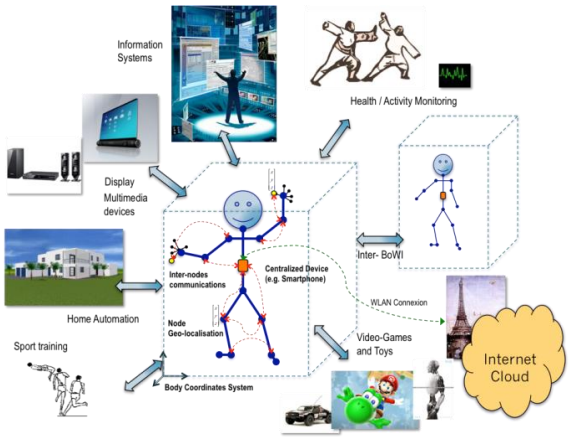

Fig. 1. BoWI concept and possible interactions.

This PhD dissertation focuses on the antennas and radio propagation part of the BoWI project which is a vital component of BoWI wireless nodes operating in close proximity to human body. Moreover, human body is considered as a hostile environment for radio due to its abnormally high tissue parameters (e.g. permittivity and conductivity) at microwave frequencies. The objective is therefore to achieve optimum radio performance for BoWI by investigating first the various radio channels in proximity to human body (e.g., on-body, off-body) and then propose miniaturized antenna solutions with stable and robust performance in proximity to body. The existing technology under discussion still suffers from many challenges and unstable antenna behavior in proximity to body due to various contributing factors such as high tissue parameters, body movement and highly dynamic body-centric radio channel in a real-time environment.

The first part of this sub-project was hence to investigate the radio channel in proximity to human body using existing front-ends for BoWI called Zyggie which comprise miniaturized chip antennas under pattern diversity configuration operating in unlicensed Industrial, Scientific and Medical (ISM) band (2.40-2.4835 GHz). In the first stage, extensive measurements were carried out for on- and off-body radio channels using the low-profile Zyggie sensors. The recorded channel data was analyzed using MATLAB® to study interesting characteristics for radio channel of BoWI such as power delay profile, delay spread, MIMO channel capacity, channel distribution etc.

2. Report structure

This report briefly describes the main achievements accomplished so far for the antennas and propagation studies for the BoWI project since the beginning of this thesis (January 2013) along with the new contributions for BAN research community. The distribution of work structure in this report is as follows.

Section 3 describes the specific prototype sensors available for the BoWI project (named as Zyggie) along with the measurement set up used for various body-centric channel measurements campaign. Section 4 deals with the off-body channel measurements carried out in a multipath indoor laboratory environment and studies important factors

such as power delay profile, delay spread and radio channel capacity. Section 5 describes a robust algorithm which was developed in MATLAB® for the selection of the best-fit distribution model for empirical radio channel data. Section 6 describes the antenna design for body-centric applications and the antenna-body interactions. The setup for numerical BAN simulations is presented in Section 7 (i.e., fixed positioning of antennas on body, and change of body posture (called alphabets) as required in BoWI project). Finally future perspective is discussed in Section 8.

3. Radio channel measurements setup

3.1.1. Zyggie sensor

For radio frequency (RF) measurements, the Zyggie sensor used in the BoWI project was modified to incorporate only the components crucial for RF (i.e., removal of the micro-controller and other on-board electronics). The modified Zyggie sensor (Fig. 2) comprises a multi-layer substrate board having two miniaturized LTCC chip antennas (monopoles) tuned in the ISM 2.4 GHz band and arranged under pattern diversity configuration. The board comprises an RF switch to select between the two antennas by mechanical opening or shortening of a jumper on-board. The switch can be powered by a 3.0 Volts DC power supply. The board provides a miniature UFL interface for access to front-end, therefore short length UFL-SMA cables (having length~10cm) were used with the Zyggie sensor for portability to SMA interface.

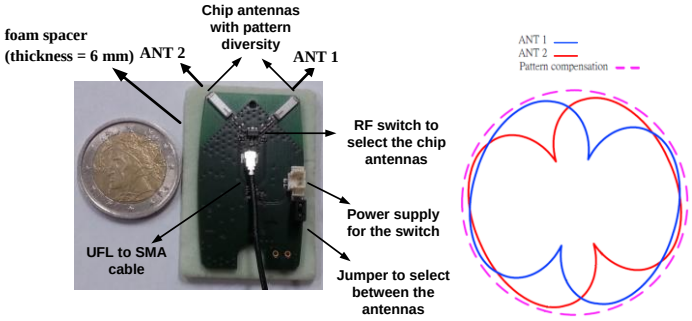

(a) (b)

Fig. 2. (a) Modified Zyggie Sensor used in the channel measurement campaign. (b) Illustration of pattern diversity offered by the orthogonal placement of antennas in (a) [1].

3.1.2. Measurement setup

The measurement setup comprises a Vector Network Analyzer (VNA) connected to a Windows PC powered by MATLAB® to control the VNA remotely using a GPIB interface. A DC power supply was used to power the switch on-board. All measured data were stored on the PC using the GPIB interface and later on, the processing of the recorded data was done offline using MATLAB®. The channel transmission coefficients were recorded with VNA during various scenarios discussed in the coming sections. Low loss cables (max. $|\hat{S}_{21}|$>-2 dB for 2-3 GHz) with characteristic impedance of 50 Ω and having length of 3.0 meter were also used between the front-end of sensors and VNA for measurements. The VNA was calibrated properly before starting each measurement campaign considering the feeding coaxial cables in order to eliminate the cable response from the measured channel coefficients. A full two-port calibration was done using standard calibration kit 85033D for the VNA model used (HP 8753ES). The two long coaxial cables (having length of 3.0 meters) were connected to the SMA interfaces of VNA and then the calibration procedures were applied directly at the ends of coaxial cables. The calibration process was also verified connecting the two ports of VNA directly through the two long cables and a negligible calibration error was observed each time (max.[abs(*error*)] = 0.05 dB for 2-3 GHz). Moreover, a VNA Tx power of 0 dBm was used throughout the measurement campaign, which is a standard value for maximum permissible power for BAN. There is no ground plane under the antennas on sensor boards, therefore foam-pad spacer (ε_r = 1) with 6 mm thickness was added under the sensor boards (Fig. 2 (a)) whenever they were used on-body to avoid detuning of antennas due to high permittivity influence of the body.

4. Off-body diversity channel measurements

In the first stage of channel measurements, off-body diversity channel was measured for analysis [2] using one Zyggie sensor on the body (chest) of a real human subject as transmitter (Tx) and another Zyggie sensor on a free space phantom (ε_r = 1) as a receiver (Rx) at a distance *d* from Tx as shown in Fig. 3. Off-body context refers to a scenario when an on-body gateway device communicates with an off-body node e.g., an access point (AP) or a base station (BS) for coordination of information. The Rx sensor was hence, used to model an AP in an off-body context.

The measurements were conducted in an indoor multipath laboratory environment, and a 177.8 cm/163 pounds adult male human subject was used as a model in the measurement campaign. Quasi-static measurement scenario was considered with the human subject in a nearly static standing body posture throughout the measurement sweep (apart from the slight involuntary breathing movements caused by the chest, hence quasi-static). A total number of 1601 points were recorded for transmission coefficients for each sub-channel S_{ij}, $(i, j) \in \{1, 2\}^2$ where i is the Tx index and j is the Rx index, for 2-3 GHz to have enough points for averaging for both line-of-sight (LoS) and non-line-of-sight (NLoS) scenarios corresponding to various distance d. Each measured response S_{ij}, $(i, j) \in \{1, 2\}^2$ contains the complex channel response in the form of real and imaginary parts.

For diversity channel analysis, a MIMO channel was constructed using the measured data for the four sub channels i.e., Tx_iRx_j, $(i, j) \in \{1, 2\}^2$. The time domain characteristics were extracted by computing the impulse response from complex Channel Transfer Function (CTF) in MATLAB®. The power delay profile (PDP) of the channel was then found by taking the spatial average of the baseband impulse response of all the four MIMO sub-channels for all frequency points (1601) between 2-3 GHz and shown in Fig. 3 (b). The PDP shows the arrival of the direct signal component followed by the multipath components for each distance for LoS where the amplitude of the direct component falls with increasing distance (~8dB/50 cm). For NLOS scenarios, Tx-Rx link was masked fully by the body as shown in the inset of Fig. 3 (b). In case of NLoS, there is mainly the multipath propagation due to the high attenuation of human tissue at microwave frequencies e.g., the attenuation constant α = 3.89 dB/cm @ 2.40 GHz for muscle tissue (ε_r = 52, σ = 1.7 Sm^{-1}) [3].

The averaged PDP was then used to compute RMS delay spread (τ_{rms}) as depicted in [4]. τ_{rms} gives the delay of multipath components, weighted proportional to their energy and hence, indicates the multipath richness of the channel. A minimum delay spread of 7.7 ns was observed for LoS (d = 50 cm) along with a maximum value of 21 ns (d = 200 cm). τ_{rms} is an important metric to limit data-rate to avoid intersymbol intereference (ISI) for multipath channels. The transmit symbol duration should be kept large enough compared to τ_{rms} (typically a factor of 10 suffices) to avoid ISI without the use of an equalizer.

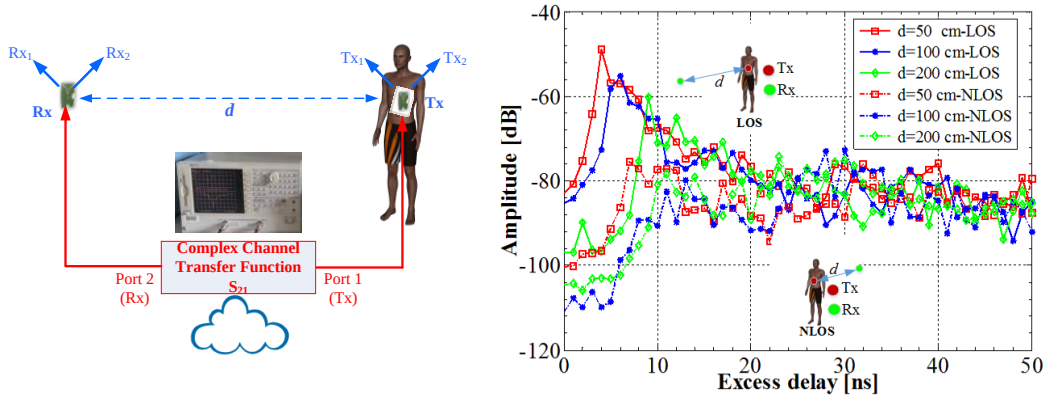

(a) (b)

Fig. 3. (a) Measurement setup. +45° orientation was considered for antennas Tx_2 and Rx_2 and -45° orientation for Tx_1 and Rx_1. (b) Average PDP of the channel computed from CTF for LoS and NLoS (scenarios shown at inside top and bottom respectively). Rx lies on free space phantom in all scenarios and Tx on-body [2].

Furthermore, the ergodic MIMO channel capacity C (bits/sec/Hz) as given in [5] was also computed constructing a 2x2 MIMO channel matrix H using the measured complex sub-channel transfer gains h_{ij}, $(i, j) \in \{1, 2\}^2$ [2]. It was assumed that the Channel State Information (CSI) is not available at the Tx i.e., the channel is completely unknown at Tx and assuming that the transmitted power is uniformly distributed among the M (=2) transmitting antennas. The MIMO channel matrix H was normalized using the Frobenius norm in order to remove the influence of power variations resulting from the path loss on the capacity computation. Thereafter, only the randomness of the multipath channel on capacity is of interest. The resulting MIMO channel capacity for the measured configuration was compared to that of the ideal channel model with independent and identically distributed (i.i.d) Rayleigh distributed and perfectly uncorrelated sub-channels.

The ergodic equal power capacity for the measured channel matrix H computed using MATLAB® is shown in Fig. 4 for both LoS and NLoS scenarios compared to that of 1x1 (SISO) and 2x2 (MIMO) i.i.d Rayleigh channels. The ergodic capacity for measured data was found by taking the average of resultant capacity matrix for each of the

samples in the frequency band 2.2-2.4 GHz. The i.i.d Rayleigh channel data was generated by MATLAB® using zero-mean, unit-variance complex Gaussian random variables.

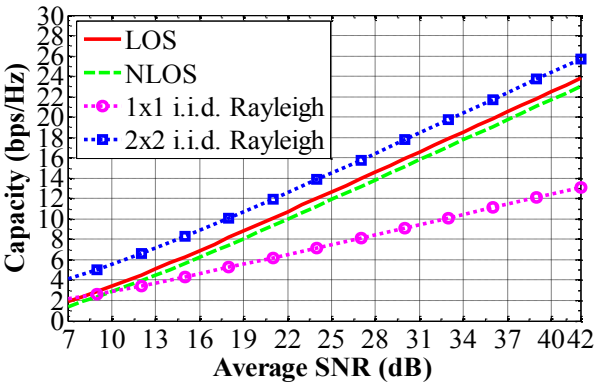

Fig. 4. Average capacity versus SNR for measurement [2] .

As depicted in Fig. 4, the proposed diversity scheme can offer improved capacity compared to SISO scheme for both LoS and NLoS configurations, especially at higher SNRs. It is also evident from Fig. 4 that the average capacity increase per 3 dB rise in SNR for our system is close to 2 bps/Hz (= min. (*M*, *N*)) which is known to be the case for an independent MIMO system in the high SNR regime [6]. Moreover, the capacity for both LoS and NLoS scenarios is quite comparable due to two main facts i.e., the channel matrix H is normalized with respect to the Frobenius norm as well as NLoS has lower correlation than LoS [5].

5. Channel distribution fitting

For system-level modeling, knowledge of the channel distribution is crucial. Distribution fitting for body-centric wireless channels has been investigated in a number of references e.g., [7], [8] and [9]. However, these citations do not refer to a systematic approach for the selection of the best distribution model in real-time scenarios where the distribution of the empirical data can fit very close to more than one standard distributions, making the selection of the best-fit a very cautious task. Therefore, we proposed and implemented a robust algorithm in MATLAB® to find the best-fit distribution model for empirical radio channel data [10]. The block diagram of the proposed algorithm is shown in Fig. 5. The algorithm is principally based on the method of MLE [11] to find the best parameter estimates for each of the attempted distributions against empirical data and further using the K-S test [12] as goodness of fit. The curve fitting was attempted with seven standard distributions i.e., Normal (*N*), Lognormal (*LG*), Rayleigh (*R*), Weibull (*W*), Gamma (*G*), Exponential (*E*) and Nakagami-*m* (*NG*) which are commonly known to hold true for wireless channel fading. The test statistics output by the algorithm are indeed based on the maximum distance between the cumulative distribution function (CDF) of fitted distribution and that of empirical one for each case. This distance between the CDFs is then used to compute the *p* value which corresponds to the probability of fitness. The idea is to choose the distribution whose CDF fits closest to that of the empirical data based on the significance level α. α was chosen as 5% which corresponds to a confidence level of 95% (=(1-α) × 100). The maximum distance between the two CDFs (i.e., empirical versus the estimated one) is used to compute the *p* value which is finally compared with the significance level to either accept or reject the null hypothesis. This is indicated by the output *h* of the algorithm. If $h = 1$, it implies that the test fails, hence rejecting the null hypothesis and indicating that the hypothesized distribution cannot be considered. However, when $h = 0$, it implies that the test fails to reject the null hypothesis, and hence the *p* value should be investigated. Finally, we set the criterion of choosing the distribution function with maximum score of *p* as the optimum fitting model for our empirical data. Such a distribution function will indeed be the one whose CDF fits closest to that of empirical data and hence, will be the optimum choice for the model stochastically.

The algorithm was validated by generating standard Normal/Gaussian random data in MATLAB and shuffling the random generator a number of times (up to one thousand) to investigate the performance of the algorithm. The algorithm successfully detected the normal distribution of the data each time with a correct mean and variance, where the *p* value of the Normal distribution always lied maximum compared to that of all the qualified distributions. However, the working principle of the algorithm is explained here with the help of one example run of the algorithm using Standard Normal data with mean $\mu = 4$ and standard deviation $\sigma = 1$. The CDF of the empirical (simulated) data along with the estimated CDFs for each distribution type using the proposed algorithm are shown in Fig. 5 (b). The corresponding test statistics output by the algorithm are also shown in Table 1. As evident from the

CDFs (inset in Fig. 5 (b)), the empirical data lies closest to the normal CDF. This is correctly reflected by the test results of the algorithm with a p value of 0.992 (along with h = 0) for Normal distribution in Table 1. Moreover, the algorithm rejects the possibility of all other distribution functions which is indicated by h =1 (and hence p = 0).

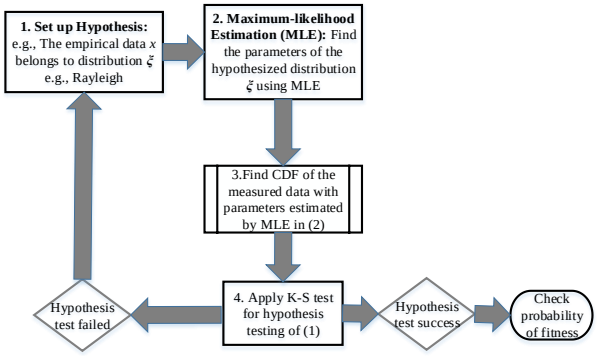

(a)

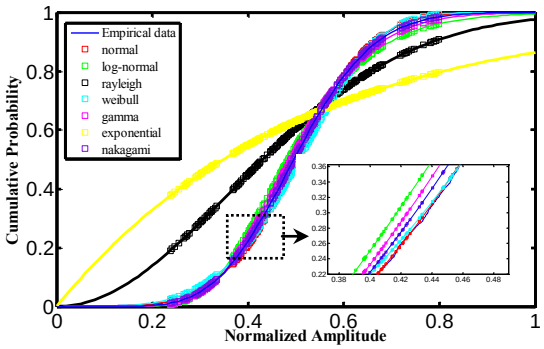

(b)

Fig. 5. (a) Block diagram of proposed fitting algorithm [10]. (b) CDF of empirical (simulated) Normal data in MATLAB for validation of algorithm. Solid curves correspond to piecewise cubic spline interpolation.

Distribution	K-S test statistic		Estimated parameters	
	h	p	μ	σ
N	0	0.992		
LG	1	0		
R	1	0	4.0017	1.0055
W	1	0		
G	1	0		
E	1	0		
NG	1	0		

Table 1. Results of channel statistics output by the fitting algorithm for simulated Normal data in Fig. 5 (b).

5.1. Off-body Channels

The fitting algorithm was then applied to find the best-fit model for small-scale first-order fading for quasi-static LoS and NLoS off-body channels. Rigorous measurement campaign was undertaken using a Zyggie sensor as Tx first on a human subject and then also on a liquid phantom modeling human tissue properties at ISM 2.4 GHz frequencies as shown in Fig. 6. The Rx in each case stayed on a free space phantom situated at a distance d from Tx. The phantom used in the experimental campaign is comprised of approximate dimensions comparable to that of human torso (44 × 25 × 21 cm^3). For LoS scenarios, the Tx and Rx faced each other without an intervening object whereas for NLoS scenarios, Tx-Rx link was masked fully by the body as indicated in Fig. 6 (b) for the case of liquid phantom. The use of such a phantom instead of a real human subject can lead to accumulation of an arbitrarily large number of points for statistical accuracy which is not realizable in the case of a human subject due to the time and patience constraints. Channel transmission coefficients were recorded at three sample frequencies within ISM band i.e., 2.40, 2.44 and 2.48 GHz for each of the measured scenarios and the transmission coefficients were recorded 1000 times for each scenario at each of the three ISM frequencies to investigate the channel temporal variations. Moreover, the Tx-Rx distance d was also varied in each case to study the variation of channel distribution. The results for two sample LoS and NLoS scenarios are shown in Fig. 7 along with the corresponding numerical data output by the algorithm for several measured scenarios shown in Table 2. Moreover, the parameters of the fitted distributions in each case are also listed in Table 2, hence fully characterizing the fitted distributions, where μ corresponds to the mean and σ is the standard deviation of Normal distribution. η is the scale parameter and β corresponds to the shape parameter of Weibull distribution and m is the shape parameter and ω is the scale parameter for Nakagami-m distribution. The graphical and numerical results were verified for all the scenarios and show excellent agreement i.e., the CDF of the distribution with maximum p value is indeed the one fitting closest to the empirical CDF. Based on the results, it can be concluded that the small-scale first-order statistics for off-body LoS channel can be best modeled by a Gaussian/Normal distribution whereas those for off-body NLoS channel can be best modeled by a Weibull distribution.

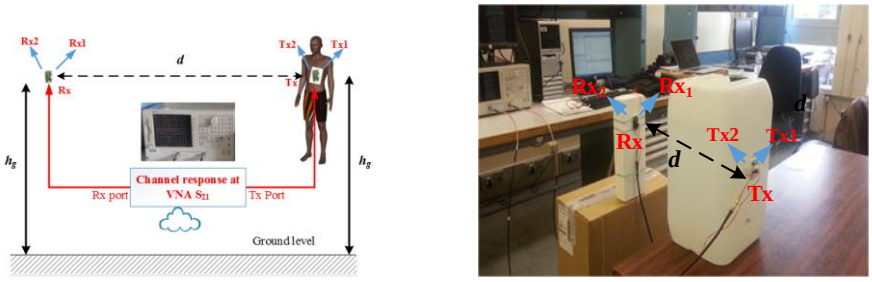

(a) (b)

Fig. 6. (a) Off-body statistical channel measurement setup representing scenarios for LoS on human subject and (b) NLoS on a liquid phantom modeling human tissue properties at ISM 2.4 GHz band [13].

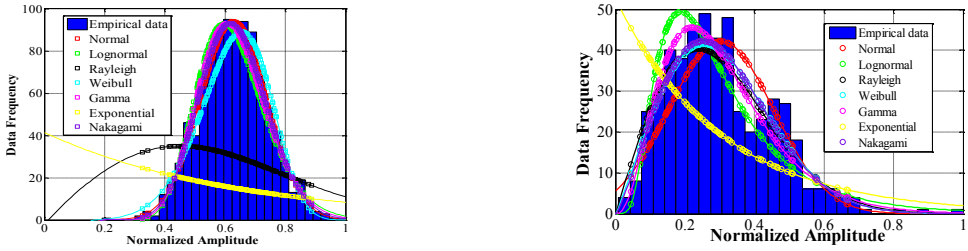

(a) (b)

Fig. 7. Probability density function (PDF) of measured empirical data against fitted distributions for (a) LoS and (b) NLoS off-body channel (Tx_2Rx_2) on human subject at 2.4 GHz and Tx-Rx distance of 100 cm.

Tx location	Link	*d* (cm)	Scenario	K-S test statistics	Distribution function							Best-Fit	Estimated parameters of Best-Fit	
					N	***LG***	***R***	***W***	***G***	***E***	***NG***			
Human subject	Tx_1Rx_1	50	LoS	***h***	0	1	1	0	1	1	0	*N*	μ = 0.6356	σ = 0.1226
				p	0.625	0	0	0.421	0	0	0.141			
			NLoS	***h***	0	1	0	0	1	1	0	*W*	η = 0.3564	β = 2.0059
				p	0.115	0	0.302	0.323	0	0	0.278			
	Tx_2Rx_2	100	LoS	***h***	0	0	1	0	0	1	0	*N*	μ = 0.6277	σ = 0.1105
				p	0.999	0.027	0	0.152	0.191	0	0.649			
			NLoS	***h***	1	1	0	0	0	1	0	*W*	η = 0.3467	β = 2.1415
				p	0	0	0.193	0.824	0.046	0	0.78			
Liquid phantom	Tx_1Rx_1	50	LoS	***h***	0	0	1	1	0	1	0	*N*	μ = 0.8129	σ = 0.0650
				p	0.552	0.155	0	0	0.256	0	0.385			
			NLoS	***h***	1	1	0	0	0	1	0	*NG*	m = 0.9878	ω = 0.1775
				p	0	0	0.926	0.944	0.04	0	0.979			
	Tx_1Rx_1	100	LoS	***h***	0	1	1	0	1	1	0	*N*	μ = 0.5349	σ = 0.1521
				p	0.864	0	0	0.423	0	0	0.0257			
			NLOS	***h***	1	1	0	0	0	1	0	*W*	η = 0.3954	β = 1.9845
				p	0	0	0.652	0.795	0.25	0	0.711			
	Tx_1Rx_2	100	LoS	***h***	0	0	1	1	0	1	0	*N*	μ = 0.8524	σ = 0.0466
				p	0.979	0.554	0	0	0.736	0	0.891			
			NLOS	***h***	0	1	0	0	1	1	0	*W*	η = 0.4087	β = 2.2560
				p	0.029	0	0.036	0.901	0	0	0.525			

Table 2. Channel statistical results output by the fitting algorithm at 2.40 GHz for various off-body channel scenarios, where *N* = Normal, *LG* = Lognormal, *R* = Rayleigh, *W* = Weibull, *G* = Gamma, *E* = Exponential, *NG* = Nakagami.

5.2. On-body Channels

The fitting algorithm was also applied for statistical study of various body-centric channel scenarios as shown in Fig. 8 using real-time measurements in a multipath indoor laboratory environment on a 177.8 cm/163 pounds adult male subject. Three on-body channels were measured for statistical study using a Zyggie sensor as Tx on the centre of chest and another Rx Zyggie sensor placed on three different positions i.e., left wrist, right thigh and back (while center-aligned with Tx on chest). The counterpart sub-channels i.e., chest to right-wrist/left-thigh, were not considered because of the inherent body symmetry. For each of the measured channels, further two scenarios were considered i.e., quasi-static and artificial walk. For quasi-static, the subject stood static throughout the measurements except the involuntary movements caused by breathing of chest (hence, quasi-static). For motion, the subject performed a slow walk on spot at a nearly constant rate with arms moving to and fro in a walk-like posture (hence, named as artificial walk). The detailed analysis of all these measured data is currently under progress. However, the CDFs and PDFs corresponding to two scenarios is shown here for reference in Fig. 9 for the sub-channel data corresponding to the three measured ISM frequencies (2.40, 2.44 and 2.48 GHz). The results output by the algorithm suggested a Weibull distribution for the scenario of chest-back channel under artificial walk scenario (Fig. 9 (a)) and a Normal distribution for chest-hip quasi-static channel as also evident from the CDF plots (Fig. 9 (b)).

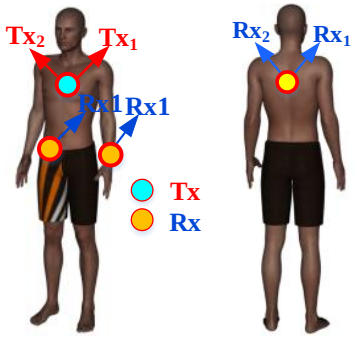

(a) (b)

Fig. 8. (a) Location of Tx/Rx Zyggie sensors for channel measurements at front and (b) back of a human subject.

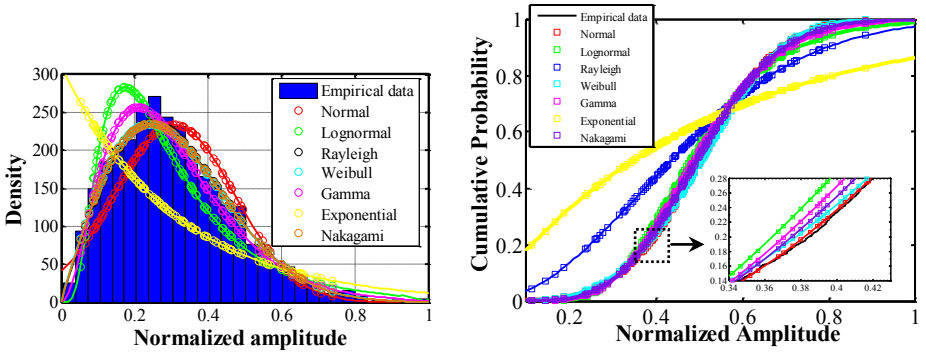

(a) (b)

Fig. 9. (a) PDF of measured empirical data vs. fitted models for chest-back channel under artificial walk scenario (b) CDF of measured empirical data vs. fitted models for chest-hip channel under quasi-static scenario (solid curves correspond to 10th degree polynomial fitting in MATLAB).

6. Antenna design

For antenna design, extensive simulation studies were done initially using CST Microwave Studio® (MWS) to investigate antenna-body interactions. Impact of human body on various antenna parameters was studied using several prototype antennas to investigate the influence of factors such as antenna-body spacing, antenna ground plane, radiation pattern and polarization. Various antenna topologies were considered and designed for ISM 2.4 GHz using CST MWS and the on-body performances were evaluated e.g., Printed Monopole (without a full ground plane), Circular Monopole (with a full ground plane), Inverted-F antenna, Meander Chip Antenna (MCA) and Short-circuited Ring Patch Antenna (SRPA). However, only two of these antenna prototypes are discussed in the following sections due to length constraints along with their on-body performance evaluations.

6.1. Meander Chip Antenna

A miniaturized meander chip antenna (MCA) was designed inspired by the one proposed in [14]. The MCA was designed and optimized using CST MWS. The laminate RO3010 having ε_r = 10.2, and h = 0.635 mm was used for size reduction (due to higher ε_r). The overall size of the designed meander chip is 9.5 x 4 x 0.635 mm^3 which corresponds to an approximate length of $\lambda/4$ at 2.40 GHz. The layout and dimensions of the optimized MCA are shown in Fig. 10. There is no ground plane under the antenna. The major electric field of the antenna is along x-axis since the currents in the meander line are aligned along x-axis whereas along y-direction the currents cancel each other, being equal and opposite. Therefore, the radiation pattern of the antenna resembles a dipole oriented along x-axis in Figure 10.

For simulation, the MCA was fed by a 50 Ω microstrip line (having width of 0.59 mm) designed on the same laminate RO3010 as MCA itself. The reflection coefficient of the antenna is represented in Fig. 11 (a) showing that the antenna resonates in the ISM 2.4 GHz band. The radiation patterns are plotted in Fig. 11 (b) and (c) showing both the co- and cross-polarization components, which correspond to E_{theta} and E_{phi} respectively. It is evident that the principal polarization of the MCA is in the theta plane (co-polarization) which is the xy plane of the coordinate system (Fig. 10 (b)). Therefore, this antenna will generate a polarization parallel to the body when placed on the human body (horizontally).

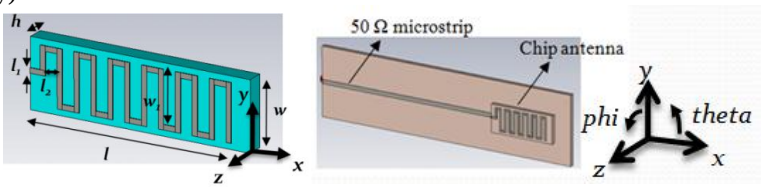

(a) (b)

Fig. 10. (a) Layout of MCA with dimensions (mm): l = 9.5, w = 4, h = 0.635, l_1= 0.3, l_2= 0.4, w_1= 3 (b) MCA with a 50 Ω microstrip matched to the antenna.

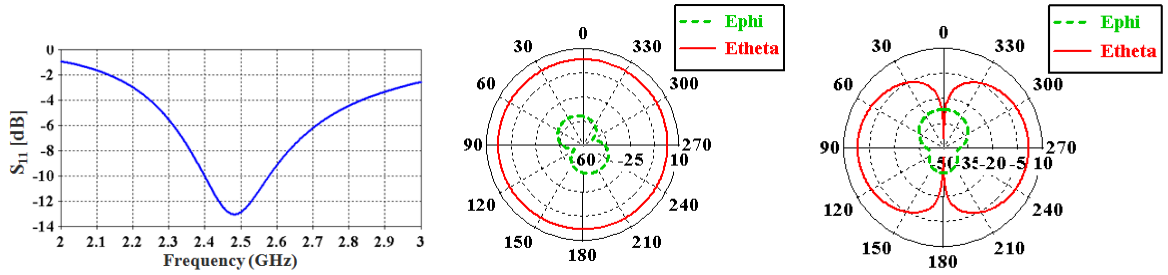

(a) (b) (c)

Fig. 11. (a) Reflection coefficient of MCA along with the microstrip feed (b) Radiation patterns in yz-plane and (c) xy-plane (coordinate system shown in Fig. 10 (b)).

6.1.1. Antenna-body Interaction

To investigate MCA interaction with the body, the antenna was placed on a dispersive homogenous body model having equivalent muscle tissue parameters i.e., ε_r = 52, σ = 1.7 S/m at 2.45 GHz with spacing (d) in CST MWS as shown in Fig. 12. PML open boundaries were used for body model in all directions (except the direction of far-field i.e., z+ in Fig. 12 (a)) to consider the worst-case antenna performance in proximity to infinite body tissue model. The reflection coefficient and radiation pattern of the antenna on body model (with d of 0.1 and 2.8 cm) are also shown in Fig. 12 compared to those in free space. A spacing of 0.1 cm was chosen as minimum instead of zero spacing due to the fact that zero spacing causes a direct contact between the microstrip ground plane and the body surface leading to a very sensitive case and hence very high losses in the antenna gain. The spacing (d) of 2.8 cm was determined to be the minimum by CST to maintain the 10-dB resonance bandwidth within ISM 2.4 GHz frequencies.

As evident from the results, the frequency is detuned for the case of d = 1 mm which is due to high permittivity of body which results in an overall increased $\varepsilon_{r,eff}$ of antenna and hence lowers the resonant frequency. The radiation patterns are also degraded in the two principal planes (Fig. 12). Moreover, the antenna patterns are more seriously degraded for a low spacing (d = 0.1 cm) in proximity to body. However for large spacing (d = 2.8 cm), the distortion

is not very crucial for the sides of the body, nevertheless the radiation is seriously attenuated in the back direction (Fig. 12 (c)) due to the attenuation caused by high σ (= 1.7 S/m) of the tissue.

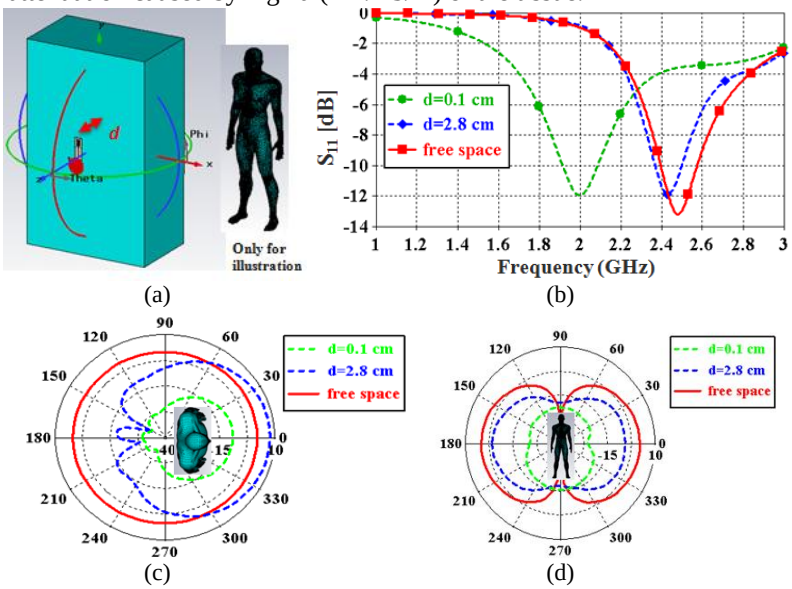

Fig. 12. (a) MCA placed on an infinite muscle tissue phantom (representative body model to show the planes for defining radiation patterns) (b) Simulated $|S_{11}|$ of MCA when placed in free space compared to on-body model with a spacing (d) of 0.1 cm and 2.8 cm (c) Radiation pattern in *xz*-plane and (c) *xy*-plane on body model for the equivalent scenarios as shown in (b).

6.2. Short-circuited Ring Patch Antenna

Another interesting antenna which has not been significantly explored yet for BAN considerations is a Short-circuited Ring Patch Antenna (SRPA). This antenna has the beauty that it is dual-mode with the first two modes being TM_{01} and TM_{11} respectively. The TM_{01} mode offers an omni-azimuthal radiation pattern just like a monopole antenna (i.e., suitable for on-body links) whereas TM_{11} mode offers radiation maximum in the broadside direction similar to a rectangular patch antenna (i.e., suitable for off-body links). The TM_{01} mode is the fundamental mode of such antenna which makes this antenna having the same omni-azimuthal type of radiation as a monopole antenna besides having an orthogonal polarization. Moreover, the antenna also includes a full ground plane. These characteristics can result in much improved on-body performance as will be proved by results. The analysis of the fundamental (TM_{01}) mode of this antenna has been done in [15].

SRPA was designed and optimized using CST MWS for first resonance in ISM 2.4 GHz band. A coaxial feed (50 Ω) was used to excite the antenna which was designed using impedance calculator macro in CST using Teflon (ε_r = 2.1) as dielectric. The overall size of the optimized antenna is 4 x 4 x 0.624 cm^3 (excluding the coax. feed). The antenna gain reaches 1.65 dBi at 2.45 GHz. The layout of the antenna is shown in Fig. 13 (a) and the reflection coefficient corresponding to two mesh refinement passes is plotted in Fig. 13 (b). These mesh passes correspond to those generated by the energy based mesh refinement criterion in CST, demonstrating the fact that the solution converges nicely with a maximum error of 0.4 % only with further mesh refinement. The 3D radiation pattern and the co- and cross-polarization patterns in the two principal planes are also represented in Fig. 14. It is evident from the results that the principal polarization of the SRPA is in the theta plane (co-polarization) which is the *xz*-plane in Fig. 13 (a). Therefore, this antenna will generate a polarization orthogonal to the body when placed on the body (horizontally).

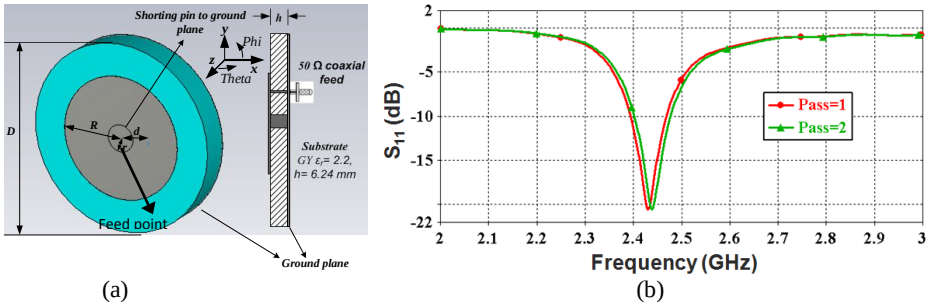

Fig. 13. (a) Layout of SRPA (dimensions (*mm*): R = 14.8, r = 4, d = 6.45, D = 40, h = 6.24) (b) Reflection coefficient showing the first resonance at 2.45 GHz (TM_{01} mode).

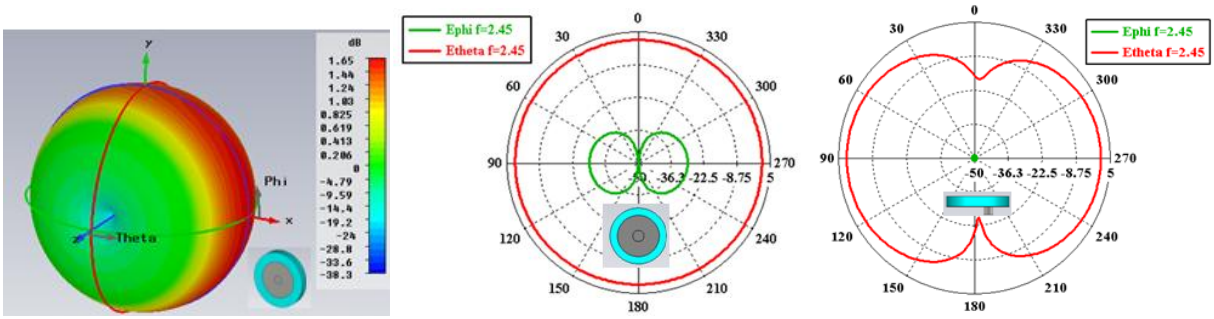

(a) (b) (c)

Fig. 14. (a) 3D far-field of SRPA (under fundamental TM_{01} mode) at 2.45 GHz (b) Radiation patterns of SRPA in *xy*-plane and (c) *xz*-plane at 2.45 GHz (Coordinate system shown in Fig. 13 (a)).

6.2.1. Antenna-body Interaction

To investigate SRPA interaction with the body, the antenna was placed on an infinite dispersive homogenous body model equivalent to muscle tissue (ε_r=52, σ =1.7 S/m at 2.45 GHz) as described in section 6.1.1, with a spacing (d) of 18 mm. The reflection coefficient and radiation patterns of the SRPA are shown in Fig. 15 for body model compared to those of free space. Both the co- and cross-polarization components (E_{theta} and E_{phi} respectively) are shown for comparison. As evident from the results, the antenna offers nearly stable performance in proximity to body for both the impedance matching and radiation characterization. Moreover, the co- and cross-polarization planes are not influenced by the body proximity i.e., the antenna offers orthogonal polarization to the body.

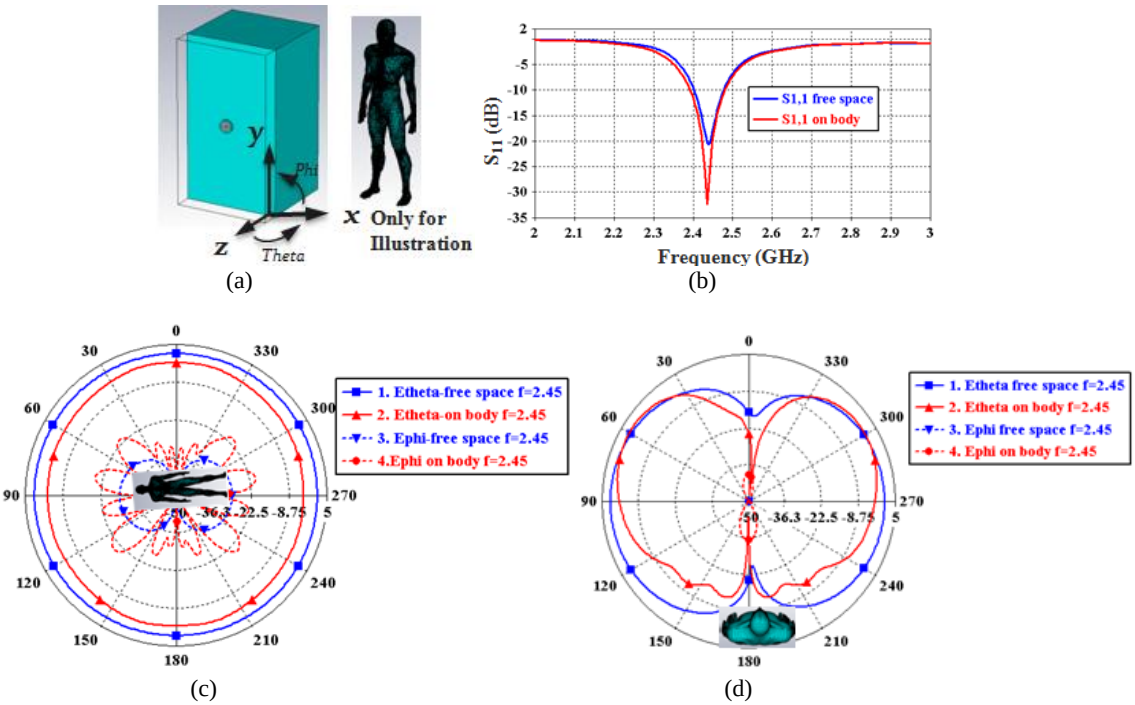

(a) (b) (c) (d)

Fig. 15. (a) SRPA on an infinite muscle tissue phantom (representative body model to show the planes for defining radiation patterns) (b) Reflection coefficient of SRPA in free space compared to on-body model for antenna body spacing (d) of 18 mm (c) Radiation pattern in *xy*-plane and (d) *xz*-plane for free space compared to on-body model for d = 18 mm at 2.45 GHz (Coordinate system shown in (a)).

7. Body-centric channel numerical studies

BoWI is based on a body-centric wireless network of various sensors at different on-body locations and further using a set of various body postures (called alphabets) to interact with the digital world. Some of such postural alphabets are shown in Fig. 16 (a)-(c). Hence, one of the prime objectives was to perform radio simulations for BoWI posture grammar to investigate the strength of various on-body links when one of the nodes communicates with another one during a specific BoWI postural alphabet. The first task was hence, to use a tool which can generate 3D body models along with the possibility to influence the body postures as desired for the BoWI posture alphabets. We investigated the BAN simulation application of some of such commercial tools as those used by artists/designers e.g., DAZ 3D® [16], POSER® [17]. These tools offer the possibility of exporting postured 3D ghost models directly in full wave simulation tools (e.g., CST MWS) for body-centric simulations. e.g., the postural alphabets produced by POSER [17] are shown in Fig. 16 (d)-(f) corresponding to the BoWI alphabets shown in Fig. 16 (a)-(c) respectively.

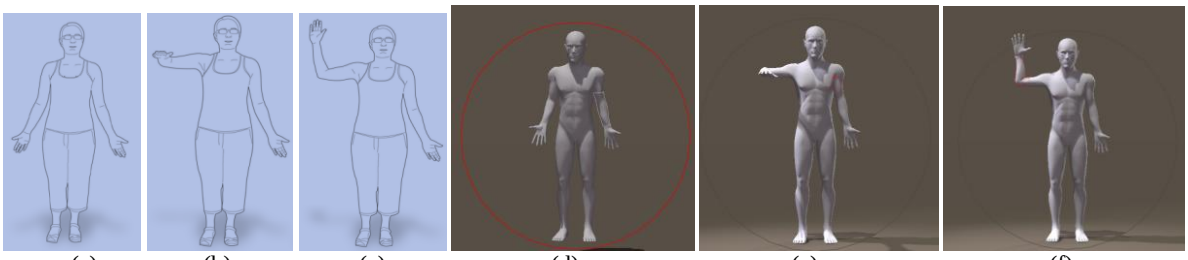

(a) (b) (c) (d) (e) (f)

Fig. 16. (a), (b), (c) Some of the sample BoWI postural alphabets (d), (e), (f) Corresponding postures generated in a commercial tool [17].

For numerical studies using different body models, the miniaturized meander chip antenna (MCA) as described in Section 6.1 was reused. After a number of extensive simulation studies using MCA under specific test scenarios on a number of such CAD based body models in CST MWS, we discovered that the choice of such models for body-centric simulations is an extremely cautious task. Our extensive study led to the discovery of the fact that many of such CAD-based body models apparently may appear solid but indeed, can be empty from inside, hence leading to erroneous or misleading results for radio simulation studies. As an example, one of the test scenarios is shown in Fig. 17 for two CAD based body models named as Model-1 [16] and Model-2 [17], which look quite similar apparently (Fig. 17 (a)). For validation of these body models, we used exactly similar NLoS scenario for both cases where one of the MCAs (as described in Section 6.1) was placed on the chest and the other MCA was placed on the back of these models. Homogeneous muscle tissue (ε_r = 52, σ = 1.7 Sm^{-1}) was used to model the human body at ISM 2.4 GHz for both cases. The E-field distribution around and inside the body in the YZ plane due to the Tx antenna is also shown in Fig. 17 (b) for body Model-1 and in Fig. 17 (c) for body Model-2. It can be seen that despite of very high tissue parameters, the *E*-field can propagate inside the body Model-1 indicating that the body Model-1 is indeed empty from inside (though apparently looks solid in CST). However for the case of Body Model-2, we can see that the attenuation of field inside the body is enormously high as expected due to the high tissue parameters (apart from a few *mm* from the body surface due to skin depth). Therefore, it proves that the selection of the CAD based body models for BAN simulations is a highly cautious task and special care must be taken when using such CAD based body models in full wave simulation tools (e.g., CST, HFSS etc.).

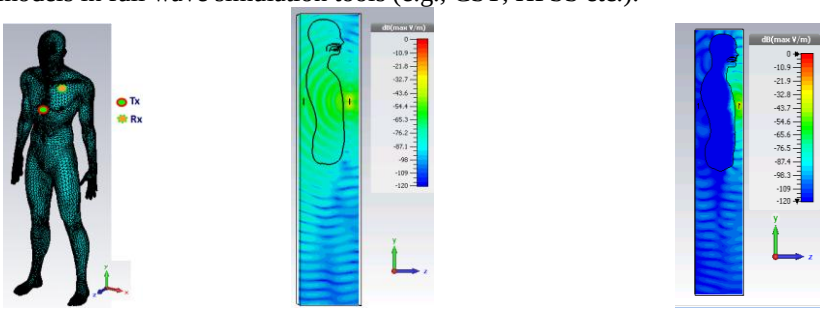

(a) (b) (c)

Fig. 17. (a) CAD based body model from a commercial tool (b) E-field distribution around and inside the body (YZ cut plane) due to Tx for Body Model-1 [16](c) E-field distribution around and inside the body (YZ cut plane) due to Tx for Body Model-2 [17].

Further using the well validated body model, we simulated a body-centric posture alphabet for BoWI (named as Neutral posture) with five nodes on the body using the miniature chip antennas as described in Section 6.1. Homogeneous muscle tissue (ε_r = 52, σ = 1.7 Sm^{-1}) was used to model the human body at ISM 2.4 GHz. A minimum antenna-body spacing of 18 mm was maintained for all the five antennas to avoid frequency detuning impact of the body due to the high permittivity value. In fact, this scenario can also lead to equivalent results for nine nodes using symmetry, when the other four nodes could be located on the left arm, while maintaining a perfect symmetry with their right-hand counterparts. Even with five nodes, such a simulation scenario is computationally quite complex due to the electrically large size of the problem (body height = 5.95 feet) and also due to the meander chip antennas which require a very fine mesh resolution for a convergent solution. This simulation problem resulted in a mesh size of 137 million approximately which took a simulation time of 33 hours approx. on a CST server with Intel Xeon 2.60 GHz CPU and 128 GB of RAM for computing 25 S-parameters in total along with the overall ***E***-field and far-field for each of the five antennas. The scenario along with some of the results is shown in Fig. 18. As expected all the S-parameters are symmetric due to the reciprocity of antennas.

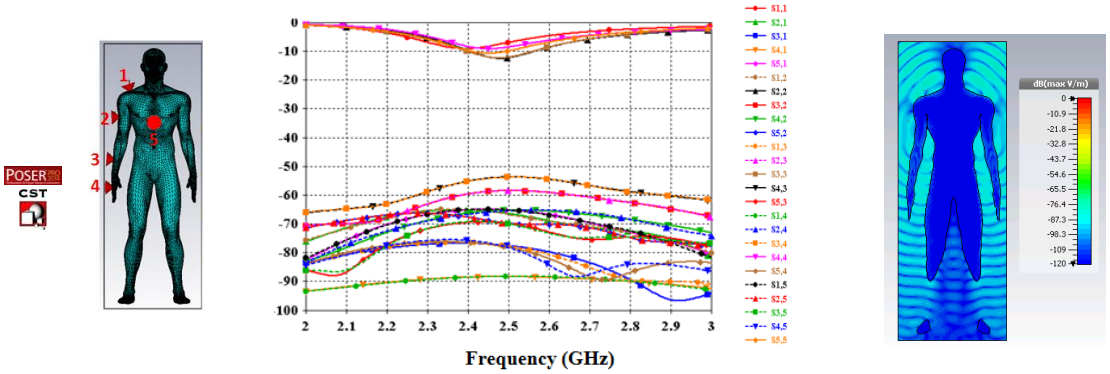

(a) (b) (c)

Fig. 18. (a) Node placement for BoWI Neutral posture (b) Scattering parameters and (c) Electric field due to antenna 5 showing on-body propagation.

The simulation challenges for another BoWI postural alphabet (named as B.1.2 and) shown in Fig. 19 (a) are discussed here. This problem posed even a much higher complexity in terms of computational size having 332 million mesh cells with five nodes compared to 137 million mesh cells for the first scenario (of Neutral posture) shown in Fig. 18. This corresponds to an increase in simulation problem complexity by a factor of 2.4. The cause of this enormous rise in computational volume is indeed the arm which lies in front of the model for this posture, hence resulting in additional mesh cells needed to simulate the volume in front of the body. Therefore, in order to reduce the problem complexity, the body model was reduced at a distance of approximately 34 cm which corresponds to $3\lambda_0$ at 2.4 GHz from the nearest antenna (antenna 5 in Fig. 19), hence resulting in 244 million mesh cells after the reduction. This simulation problem took a simulation time of 56 hours approx. on a CST server with Intel Xeon 2.60 GHz CPU and 128 GB of RAM for computing 25 S-parameters in total along with the E-field for each of the five antennas. The scenario along with the simulated S-parameters is shown in Fig. 19. Moreover, the results for the case when there are also four more antennas on the left arm for this posture (i.e., nine antennas in total) will be analogous to those of the Neutral posture alphabet, when a perfect symmetry is maintained with the placement of the four antennas on the left arm of this posture with their right-hand counterparts of the Neutral posture.

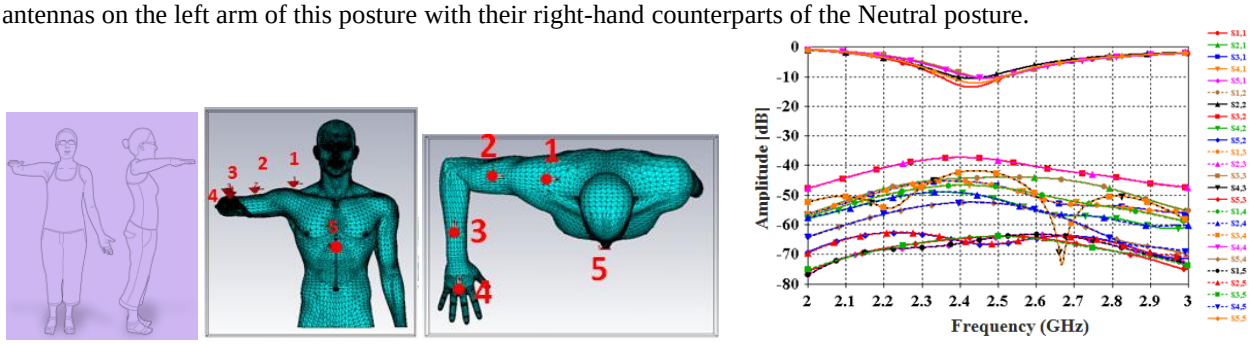

(a) (b) (c)

Fig. 19. (a) BoWI posture alphabet (B.1.2) (b) Node placement for the posture (front- and top views) (c) Scattering parameters for all five antennas.

Our simulation setup as discussed above also provides a large number of possibilities for BAN simulation studies utilizing a number of well-validated body model postures along with various antenna configurations for interesting antenna and radio channel studies.

8. Perspective Work plan

- Exploration of pattern and polarization diversities using the two standard types of radiation and polarization scenarios known for optimal BAN performance i.e.,
  - an omni-azimuthal radiation with orthogonal polarization to body (known to be suitable for on-body scenarios).
  - a broadside radiation with a polarization parallel to the body (known to be suitable for off-body scenarios).
- Numerical study of these scenarios on sample BoWI posture alphabets to investigate link performances.
- Design and experimental characterization of a pattern/polarization diversity antenna.

9. Publications (Jan . 2013 to date)

[2], [10] and [13]

Bibliography

[1] "http://johansontechnology.com/," [Online].

[2] R. Masood, R. Burghelea, A. Carer, M. Le Gentil, O. Sentieys, P. Pajusco, C. Person, and R. Sauleau, "Indoor Off-Body Channel Measurements using miniaturized Chip Antennas with Pattern Diversity," in *European Microwave Conference (EuMC)*, Rome, Italy, 5-10 Oct. 2014.

[3] I. Yamaura, "Measurements of 1.8 - 2.7-Ghz Microwave Attenuation in the Human Torso," *IEEE Transactions on Microwave Theory and Techniques*, vol. 25, no. 8, pp. 707-710, Aug. 1977.

[4] P. Pagani, F. T. Talom, P. Pajusco, and B. Uguen, Ultra Wideband Radio Propagation Channels : A Practical Approach, Wiley, 2008.

[5] I. Khan and P S. Hall, "Experimental evaluation of MIMO capacity and correlation for narrowband body-centric wireless channels," *IEEE Transactions on Antennas and Propagation*, vol. 58, no. 1, pp. 195-202, Jan. 2010.

[6] E. Biglier, R. Calderbank, A. Constantinides, A. Goldsmith, A. Paulraj, and H. V. Poor, MIMO Wireless Communications, New York: Cambridge Univ. Press, 2007.

[7] Q.H. Abbasi, M. M. Khan, S. Liaqat, A. Alomainy, and Y. Hao, "Ultra wideband off-body radio channel characterization for different environments," in *7th International Conference on Electrical & Computer Engineering (ICECE)*, Dec. 2012.

[8] D. Smith, L. Hanlen, J. Zhang, D. Miniutti, D. Rodda, and B. Gilbert, "Characterization of the dynamic narrowband on-body to off-body area channel," in *IEEE Int. Conf. on Communications*, Jun. 2009.

[9] M. M. Khan, Q. H. Abbasi, A. Alomainy, and Y. Hao, "Radio propagation channel characterisation using ultra wideband wireless tags for body-centric wireless networks in indoor environment," in *International Workshop on Antenna Technology (iWAT)*, Hong Kong , Mar. 2011.

[10] R. Masood, C. Person, and R. Sauleau, "Distribution Fitting for Real-Time off-Body Channel Measurements," in *IEEE International Microwave Workshop Series on RF and Wireless Technologies for Biomedical and Healthcare Applications*, London, UK, 8-10 Dec. 2014.

[11] M. Evans, N. Hastings, and B. Peacock, Statistical Distributions, 2nd edition, Wiley, 1993.

[12] F. J. Massey, "The Kolmogorov-Smirnov Test for Goodness of Fit," *Journal of the American Statistical Association*, vol. 46, no. 253, pp. 68-78, 1951.

[13] R. Masood, C. Person, R. Sauleau, and P. Pajusco, "Ajustements statistiques pour l'étude du canal off-body en configuration NLoS à 2,4 GHz," in *XIXèmes Journées Nationales Microondes*, Bordeaux, France, Jun. 2015 (submitted for publication).

[14] W. Choi, S. Kwon, B. Lee, "Ceramic chip antenna using meander conductor lines," *Electronics Letters*, vol. 37, no. 15, pp. 933-934, 2001.

[15] V. G. Posadas, D. S. Vargas, E. R. Iglesias, J.L. Vazquez-Roy, C. M. Pascual, "Approximate analysis of short circuited ring patch antenna working at TM01 mode," *IEEE Transactions on Antennas and Propagation*, vol. 54, no. 6, pp. 1875-1879, Jun. 2006.

[16] "www.daz3d.com," [Online].

[17] "http://my.smithmicro.com/," [Online].